JOURNAL OF AIRCRAFT
Vol. 37, No. 6, November–December 2000

Transition of Subsonic and Transonic Expansion-Corner Flows

Kung-Ming Chung*
National Cheng-Kung University, Tainan 711, Taiwan, Republic of China

A naturally developed turbulent boundary layer past convex corners was studied. Attention is on the transition of subsonic and transonic expansion flows. Convex-corner angle α ranges from 5 to 20 deg, and freestream Mach numbers M_∞ are 0.33, 0.64, and 0.83. Reynolds numbers based on the incoming boundary-layer thickness $Re_{\delta 0}$ are 10.0, 14.9, and 16.8 $\times 10^4$, respectively. Transition of subsonic and transonic expansion-corner flow is observed at $M_\infty^2\,\alpha = 6.14$. The sudden expansion near the corner is also scaled with this parameter at $M_\infty = 0.64$ and 0.83, but not for $M_\infty = 0.33$.

Nomenclature

C_p = pressure coefficient, $(p_w - p_\infty)/q_\infty$
M_∞ = freestream Mach number
p = pressure
q_∞ = dynamic pressure
Re = Reynolds number
U = velocity
x = coordinate along the surface of the corner
x^* = normalized streamwise distance, x/δ_0
α = convex-corner angle, deg
δ_0 = incoming boundary-layer thickness ($x = -35$ mm)

Introduction

AIRCRAFT designs have employed flaps for takeoff and landing performance and ailerons for routine turning maneuvers. With developing technology in transonic aerodynamics, the aerodynamists began with in-depth studies of camber optimization in the 1970s. A previous study indicated that active modification of control surfaces potentially could play a role in performance optimization for fighter aircraft and current- and future-generation transport aircraft.[1] Deflected control surfaces, such as flaps and ailerons, can be used in combination to provide variable-camber control during cruise flight. In general, increasing camber at the trailing edge of a transonic wing could result in higher lift at constant angle of attack, higher buffet boundary, and increasing pitching moment. A study by Szodruch and Hilbig[2] further indicated that the critical Mach number, onset of boundary-layer separation, and drag are strongly related to the deflection of control surfaces (or camber). However, a conventional highly loaded transonic airfoil usually has a large supersonic region, a general tendency toward strong reexpansion downstream of the shock wave, and a steep pressure gradient near the trailing edge. The boundary layer is weakened considerably so that small deflection of flaps can evoke separation.[3] Thus although deflection of control surfaces can be used to obtain maximum performance of an aircraft, there exists a great deal of uncertainty regarding the allowable deflection before separation near the hinge line.[4]

The present study examines the subsonic and transonic convex-corner (or expansion) flows (Fig. 1). This is an idealized configuration that models the deflection of a control surface at off-design conditions. The general characteristics of the flowfield include sudden expansion near the corner followed by recompression. In general, the flowfield is a pure expansion and recompression type at lower Mach number. At higher Mach number the flow may expand to supersonic velocity. The subsonic expansion flow is switched to a transonic expansion flow. Recompression occurs through a shock wave. As the Mach number or convex-corner angle increases further, the shock wave separates the boundary layer. A study of Mason[4] indicated that there are two fundamental issues regarding this convex-corner flow. It is known that scale effect (or Reynolds number) is important for the onset of boundary-layer separation. A high Reynolds number will maintain a stronger adverse pressure gradient than that of the lower Reynolds number. Because of the limit of the facility, the effect of Reynolds number is not included in this study. Another key issue is the condition under which the flow switches from subsonic to transonic type. For the present study the effects of convex-corner angle and freestream Mach number on the transition criterion are investigated. Before discussing the results of the present study, brief details of the experiment are outlined next.

Experiment

Transonic Wind Tunnel

ASTRC/NCKU transonic wind tunnel is a blowdown-type wind tunnel.[5] The operating Mach number ranges from 0.2 to 1.4, and the simulated Reynolds number is up to 20 million per meter. The major components of the facility include compressors, air dryers, cooling water system, storage tanks, and the tunnel. Dew point of high-pressure air through the air dryers is maintained at -40°C under normal operation conditions. Air storage volume for three storage tanks is up to 180 m^3 at 5.15 MPa. The 600-mm square test section is 1500 mm long. In the present study the test section is assembled with solid sidewalls and perforated top/bottom walls. Testing freestream Mach numbers M_∞ are 0.33, 0.64, and 0.83 ± 0.01. Also for all of the tests, stagnation pressure p_0 and stagnation temperature T_0 are 172 ± 0.5 kPa and room temperature, respectively.

For the data acquisition systems a NEFF 620 Instruments System and a LeCroy data acquisition system are available. The test conditions are recorded by the NEFF system, whereas the LeCroy 6810 waveform recorders are used for surface-pressure measurements. A host computer with CATALYST software controls the setup of LeCroy waveform recorders through a LeCroy 8901A interface. All input channels are triggered simultaneously by using an input channel as trigger source.

Test Model

The upstream boundary layer is developed along a long flat plate in the test section. The plate with a 4-deg sharp leading edge is 150 $\times$ 450 mm and is supported by a single sting mounted on bottom wall of the tunnel. For the surface-pressure measurements seven instrumentation plates with 0, 5, 10, 13, 15, 17, and 20 deg $\pm$ 0.1 deg convex angle are fabricated. The instrumentation plates are 150 $\times$ 150 mm, where the corner is located at 500 mm from the leading edge of the flat plate. One row of 19 pressure taps, 6 mm apart and 2.5 mm in diameter, along the centerline of each plate is drilled perpendicularly to the test surface. Side fences at both sides of the instrumentation plate are used to prevent crossflow. This

Received 26 January 2000; revision received 29 May 2000; accepted for publication 1 June 2000.

*Associate Research Fellow, Aerospace Science and Technology Research Center, 198 Shin-Sheng Street, Kueijen. Senior Member AIAA.

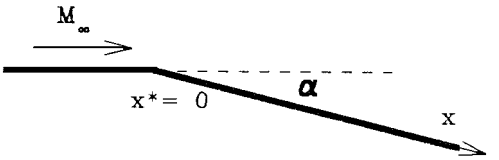

Fig. 1 Test configuration.

investigation covers the cases where there is no separation and cases where the boundary layer is extensively separated.

Experimental Techniques

Pressure transducers used for the surface-pressure measurements are Kulite dynamic pressure transducers, Model XCS-093-25A (B screen). The outside diameter is 2.36 mm, and the sensing element is 0.97 mm in diameter. Natural frequency is 200 kHz as quoted by the manufacturer. For surface-pressure measurements all of the pressure transducers are potted using silicone rubber sealant, and the flushness is checked by a machinist's block to minimize interference with the flow. In addition, all of the pressure transducers are powered by a TES Model 6102 power supply at 15.0 V. External amplifiers (Ecreon Model E713, 12 channels) are also used. With a gain of 20, the roll-off frequency is about 140 kHz. A typical sampling rate for all of the tests is 200 ksamples/s (or 5 μs). Each test record samples 131,072 data points for statistical analysis. The data are divided into 32 blocks. Mean values of each block (4096 data points) are calculated. Variation of the blocks is estimated to be 0.43% for the pressure coefficient C_p, which is considered as the uncertainty of experimental data.

For the pitot-pressure surveys a Kulite pressure transducer (Model XCS-093-25A) is installed inside a probe at 20 mm from the tip to ensure a fast response. The flattened intake is 2.0 mm wide $\times$0.3 mm high to minimize the displacement effect. A one-dimensional traversing mechanism is also used to move the pitot probe vertically. Incoming boundary-layer surveys are conducted at 465 mm from the leading of the flat plate (or equivalent to 35 mm upstream of the corner). Normalized velocity profiles appear to be full ($n \approx 7$–11 for the velocity power law). These indicate turbulent flow at the measurement locations. The Reynolds number based on the incoming boundary-layer thickness $Re_{\delta 0}$ is 10.0, 14.9, and 16.8 $\times 10^4$ for Mach 0.33, 0.64, and 0.83, respectively.

Result and Discussion

Surface-Pressure Distributions

Mean surface-pressure distributions on the centerline of the instrumentation plates normalized by the stagnation pressure p_0 are plotted in Figs. 2–4 for seven test cases at $M_\infty = 0.33, 0.64$, and 0.83, respectively. The origin of the x coordinate is set at the corner. At $M_\infty = 0.33$, Fig. 2, the mean surface-pressure distributions appear similar in shape for all of the convex-corner test cases. The flows accelerate upstream of the convex corner and reach the minima just downstream of the corner. Upstream expansion occurs as a result of the displacement thickness on the effective local wall surface. Then the flows decelerate immediately after the corner (recompression), and the levels of mean surface pressure tend to equilibrium values at further downstream locations. The flowfield appears to be a pure expansion and recompression type (or subsonic expansion flow). The observation is also made that there are stronger upstream expansions and steeper downstream recompressions with increasing convex-corner angle. This may imply that the boundary layer upstream of the corner becomes thin and approaches the case of inviscid flow[4] at a larger convex-corner angle. For $M_\infty = 0.64$, Fig. 3, the flow is still subsonic for $\alpha \leq 15$ deg. However, larger favorable and adverse pressure gradients near the corner are observed compared with those at $M_\infty = 0.33$. At $\alpha = 17$ and 20 deg stronger upstream expansions are seen, and the flows expand to supersonic speed immediately downstream of the corner, where $p_w / p_0 = 0.528$ corresponds to the sonic condition. This indicates that the expansion flow switches from the subsonic to the transonic type. At further

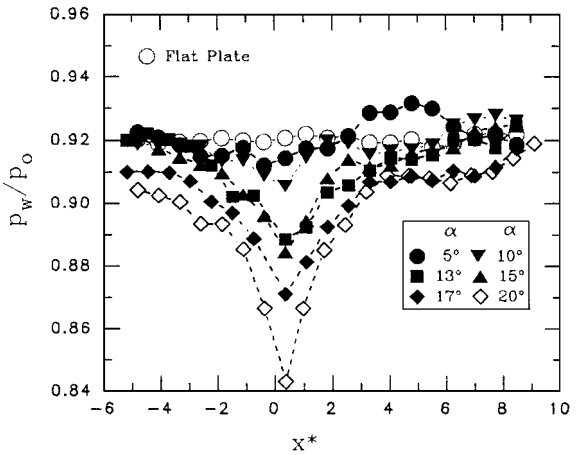

Fig. 2 Mean surface-pressure distributions, $M_\infty = 0.33$.

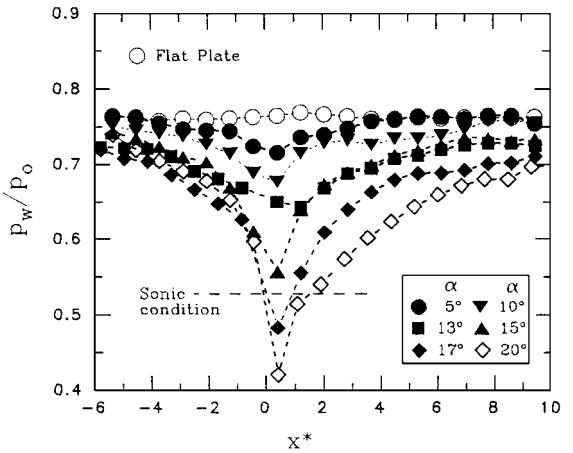

Fig. 3 Mean surface-pressure distributions, $M_\infty = 0.64$.

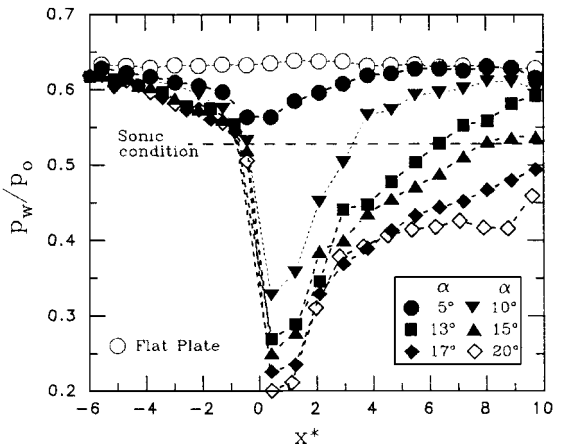

Fig. 4 Mean surface-pressure distributions, $M_\infty = 0.83$.

downstream locations the flows return to subsonic condition during the recompression. This pressure distribution pattern indicates that there is only a single shock produced under these test conditions, and the initial compression is just underneath the shock foot.[6] Further, the observation is made that the type of transonic expansion flow results in a much milder return to the final equilibrium condition, as happened in the case of $M_\infty = 0.64$ and $\alpha = 20$ deg. For the cases of $M_\infty = 0.83$, the flows expand to supersonic speed except for the case of $\alpha = 5$ deg. The upstream expansions are nearly the same at larger convex-corner angles. It means that a further increase of the convex-corner angle has a minor effect on the pressure distributions upstream of the sonic line. Downstream of the corner, the

pressure variation is much less severe at the initial recompression, Fig. 4. The flows remain at a supersonic condition within the initial recompression. This implies that the single shock-wave pattern can switch to a lambda shock-wave pattern,[6] in which the initial recompression is related to the leading oblique shock wave. At a larger convex-corner angle ($\alpha \geq 15$ deg) the mean surface-pressure distributions indicate that the flows still remain supersonic within the measurement locations. It suggests that the shock wave is more oblique and a Mach reflection can form under these test conditions. Moreover, it is found that there is a distinctive kink of mean surface-pressure distribution at $x^* \approx 2.5$ for $\alpha = 13$ deg. This indicates that the shock wave separates the boundary layer, which is also observed from oil-flow visualizations.[7] Further downstream of the corner, the flow is compressed and returns to subsonic through the reattachment process. For $\alpha \geq 15$ deg a slow recovery process is observed associated with a more extensively separated boundary layer.

Mach-number distributions based on the isentropic relations are shown in Figs. 5–7. For the cases of transonic expansion flows, there is some variation of stagnation pressure through the shock wave. The isentropic Mach number M_{is} must be used with caution. In general, it can be seen that the flow expands suddenly and reaches a peak Mach number M_p near the corner. For cases with high peak Mach number, e.g., $M = 0.83$ and $\alpha \geq 15$ deg, there is a short region of mild variation of Mach number followed by a sharp Mach-number drop. This region of mild Mach-number variation is considered as the region of initial recompression. Also, the sharp Mach-number drop is roughly the same ($\Delta M \approx 0.23$) for the three test cases ($\alpha = 15$, 17, and 20 deg). No explanation for the effect is known at this time.

Transition Criterion

The minimum surface-pressure coefficients $C_{p,\min}$ immediately downstream of the corner are summarized in Fig. 8 for all of the test cases, where the pressure coefficient $C_{p,\min}$ is plotted against the convex-corner angle α. $C_{p,\min}$ decreases with increasing α and M_∞. Expansion of the flows show some linear variation with α but not with M_∞. Further, M_∞ and α are the two major parameters affecting the type of flowfield. Thus the hypersonic similarity parameter[8] ($M_\infty \alpha$) and a similar combined supersonic–hypersonic similarity parameter[9] [$\sqrt{(1 - M_\infty^2)}\alpha$] were examined for scaling the expansion flows. However, these parameters were found to be not applicable for the present test conditions. On the other hand, the parameter $M_\infty^2 \alpha$ appears to be suitable. In the present study $M_\infty^2 \alpha$ ranges from 0.54 to 13.78. A correlation of $C_{p,\min}$ with $M_\infty^2 \alpha$ is shown in Fig. 9. The expansions near the corner at higher freestream

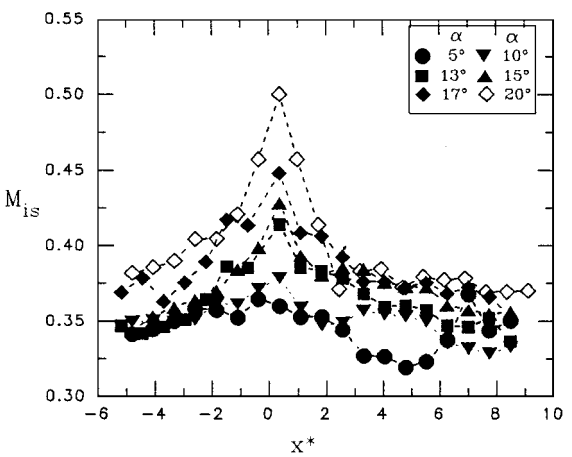

Fig. 5 Isentropic Mach-number distributions, $M_\infty = 0.33$.

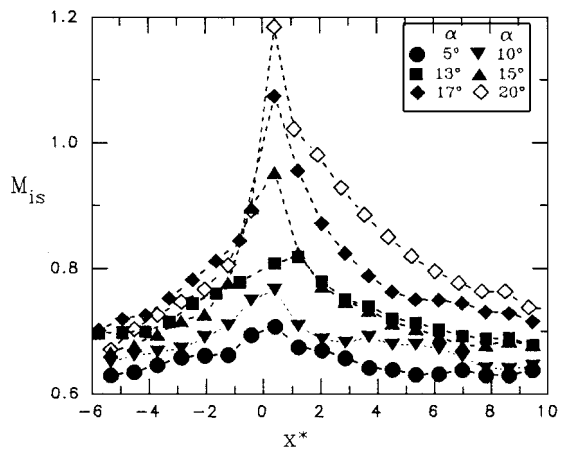

Fig. 6 Isentropic Mach-number distributions, $M_\infty = 0.64$.

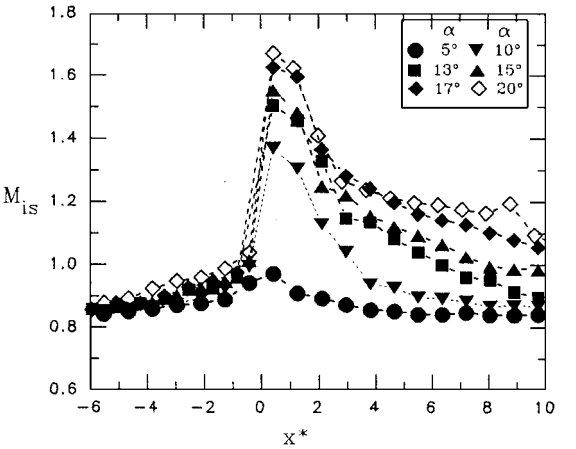

Fig. 7 Isentropic Mach-number distributions, $M_\infty = 0.83$.

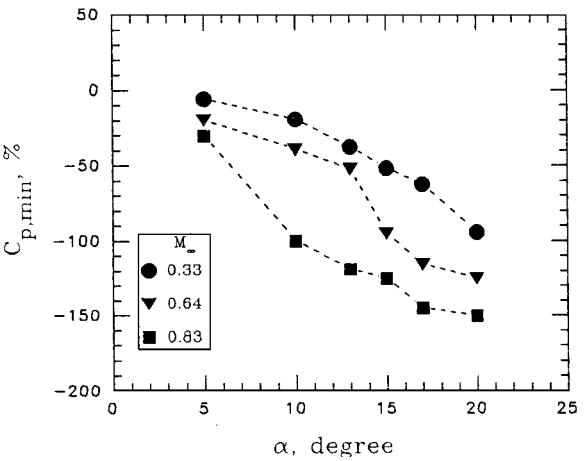

Fig. 8 Minimum pressure coefficients.

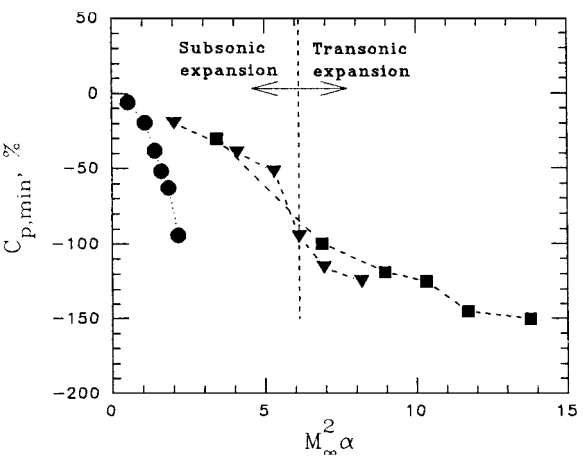

Fig. 9 Minimum pressure coefficient with $M_\infty^2 \alpha$.

Mach numbers ($M_\infty = 0.64$ and 0.83) collapse reasonably well with $M_\infty^2 \alpha$. However, it also shows that the correlation is not applicable at a lower Mach number ($M_\infty = 0.33$). This is reasonable because of the compressibility effect on upstream boundary-layer development and the type of expansion flow. Further, the slope of $C_{p,\min}$ vs $M_\infty^2 \alpha$ changes significantly at $M_\infty^2 \alpha = 6.14$, which corresponds to a local Mach number of 0.96 at $x^* = 0.38$. Because there is no data point at the corner, the maximum local Mach number cannot be obtained. However, it is suggested that the flow switches from a subsonic expansion to a transonic expansion under this test condition.

The peak Mach numbers M_p for all of the test cases are summarized in Fig. 10. It shows that M_p increases with increasing α and M_∞. Expansion near the corner is more pronounced at higher freestream Mach numbers ($M_\infty = 0.64$ and 0.83) than at a lower Mach number ($M_\infty = 0.33$). For the transonic expansion flows, M_p reaches 1.67 in front of the shock wave under the present test conditions. M_p normalized by the freestream Mach number M_∞ is plotted against the parameter $M_\infty^2 \alpha$ in Fig. 11, where a good correlation of the normalized peak Mach number with $M_\infty^2 \alpha$ at higher freestream Mach numbers is shown. A transitional behavior between subsonic and transonic expansions is observed at $M_\infty^2 \alpha = 6.14$.

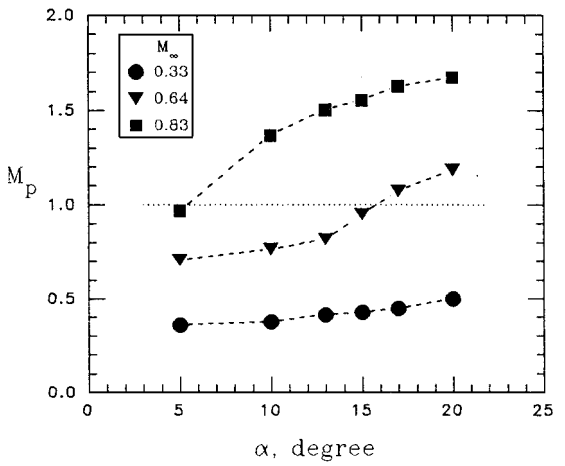

Fig. 10 Peak Mach number.

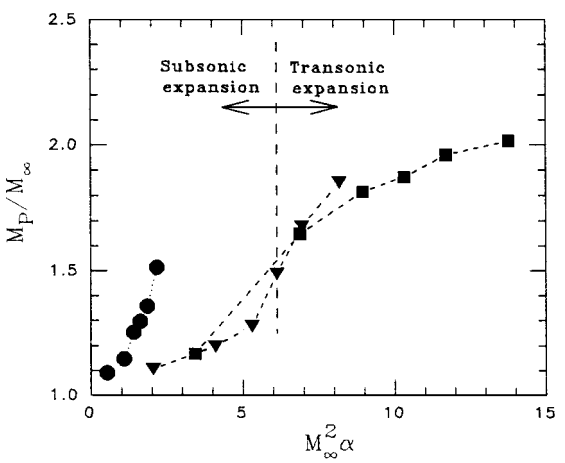

Fig. 11 Normalized peak Mach number with $M_\infty^2 \alpha$.

Conclusions

Experiments are carried out to study the transition of subsonic and transonic expansion flows. At a given freestream Mach number the mean surface-pressure distributions show that deflection of the physical wall surface has a strong effect on the structure of the flow pattern, which can include an attached flow, a single shock-wave pattern, a lambda shock-wave pattern, or a possible Mach reflection. A typical pure subsonic expansion flow results in an upstream expansion and a downstream recompression near the corner. As the freestream Mach number or convex-corner angle increases, stronger expansions and steeper recompressions are observed. The steeper recompression implies that the boundary layer is thinning and the flow can approach the inviscid case. At higher freestream Mach number and larger convex-corner angle, the flow switches from a subsonic expansion flow to a transonic expansion flow. The critical parameter $M_\infty^2 \alpha$, where this occurs, is about 6.14. The minimum pressure coefficient and peak Mach number near the corner can be scaled with $M_\infty^2 \alpha$ at higher freestream Mach numbers.

Acknowledgments

This research was supported by National Science Council (88-2612-E-006-004). The support is gratefully acknowledged. The author also thanks the technical support of ASTRC/NCKU technical staffs with the experiments.

References

[1] Bolonkin, A., and Gilyard, G. B., "Estimated Benefits of Variable-Geometry Wing Camber Control for Transport Aircraft," NASA TM-1999-206586, Oct. 1999.

[2] Szodruch, J., and Hilbig, R., "Variable Wing Camber for Transport Aircraft," *Progress in Aerospace Science*, Vol. 25, No. 3, 1988, pp. 297–328.

[3] Greff, E., "Aerodynamic Design and Integration of a Variable Camber Wing for a New Generation Long/Medium Range Aircraft," International Council of the Aeronautical Sciences, Paper 88-2.2.3, Aug. 1988.

[4] Mason, W. H., "Fundamental Issues in Subsonic/Transonic Expansion Corner Aerodynamics," AIAA Paper 93-0649, Jan. 1993.

[5] Chung, K. M., "Calibration of ASTRC/NCKU 600 mm × 600 mm Transonic Wind Tunnel," National Science Council, NSC 83-0424-E-006-141T, Taiwan, ROC, Jan. 1994.

[6] Liu, X., and Squire L. C., "An Investigation of Shock/Boundary Layer Interactions on Curved Surfaces at Transonic Speeds," *Journal of Fluid Mechanics*, Vol. 187, Feb. 1988, pp. 467–486.

[7] Chung, K. M., "Investigation on Transonic Shock Wave and Boundary Layer Interaction," National Science Council, NSC 87-2212-E-006-020, Taiwan, ROC, Dec. 1998.

[8] Lu, F. K., and Chung, K. M., "Downstream Influence Scaling of Turbulent Flow Past Expansion Corners," *AIAA Journal*, Vol. 30, No. 12, 1992, pp. 2976, 2977.

[9] Van Dyke, M. D., "The Combined Supersonic and Hypersonic Similarity Rule," *Journal of the Aeronautical Sciences*, Vol. 18, No. 7, 1951, pp. 499, 500.